Editors' Suggestion

Universal Features of Entanglement Entropy in the Honeycomb Hubbard Model

Jonathan D'Emidio,[1,*] Román Orús,[1,2,3] Nicolas Laflorencie,[4,1] and Fernando de Juan[1,2]
[1]Donostia International Physics Center, P. Manuel de Lardizabal 4, 20018 Donostia-San Sebastián, Spain
[2]IKERBASQUE, Basque Foundation for Science, Maria Diaz de Haro 3, 48013 Bilbao, Spain
[3]Multiverse Computing, Paseo de Miramón 170, E-20014 Donostia-San Sebastián, Spain
[4]Laboratoire de Physique Théorique, Université de Toulouse, CNRS, UPS, 31400 Toulouse, France

(Received 12 January 2023; revised 18 December 2023; accepted 26 January 2024; published 14 February 2024)

The entanglement entropy is a unique probe to reveal universal features of strongly interacting many-body systems. In two or more dimensions these features are subtle, and detecting them numerically requires extreme precision, a notoriously difficult task. This is especially challenging in models of interacting fermions, where many such universal features have yet to be observed. In this Letter we tackle this challenge by introducing a new method to compute the Rényi entanglement entropy in auxiliary-field quantum Monte Carlo simulations, where we treat the entangling region itself as a stochastic variable. We demonstrate the efficiency of this method by extracting, for the first time, universal subleading logarithmic terms in a two-dimensional model of interacting fermions, focusing on the half-filled honeycomb Hubbard model at $T = 0$. We detect the universal corner contribution due to gapless fermions throughout the Dirac semi-metal phase and at the Gross-Neveu-Yukawa critical point, where the latter shows a pronounced enhancement depending on the type of entangling cut. Finally, we observe the universal Goldstone mode contribution in the antiferromagnetic Mott insulating phase.

DOI: 10.1103/PhysRevLett.132.076502

The entanglement entropy (EE) quantifies the information shared between a subsystem and its environment in a quantum many-body wave function. Remarkably, the EE finite-size scaling form has contributions that depend uniquely on universal physical quantities, making it a powerful probe to characterize strongly correlated systems. A famous example of this is found in one-dimensional critical systems, where the EE grows logarithmically in the subsystem size with a prefactor given by the central charge [1–4]. In two dimensions the EE grows in proportion to the boundary of the subsystem, the so-called "area law" [5], but critical ground states display a subleading universal logarithmic contribution when the subsystem contains sharp corners [6,7]. Additionally, in the case of continuous symmetry breaking, each Goldstone mode contributes a logarithmic term with a coefficient equal to one half [8–10]. In the absence of symmetry breaking, topological states can be detected by a universal negative constant term in the EE [11,12] as well as other entanglement measures [13,14].

Despite a wide variety of numerical work investigating spin and boson systems [15], the universal features of EE of 2D interacting fermions have largely remained an unexplored frontier. Important exceptions have focused on the universal constant in gapped systems, as in the case of the topological EE of fractional quantum hall ground states [16,17] and angle dependent constant of the $\nu = 1/2$ Laughlin wave function [18]. Additionally, the flux dependence of the constant term for gapless Dirac fermions was investigated in [19].

Since the pioneering work of Grover [20], auxiliary-field determinental quantum Monte Carlo (DQMC) simulations have offered a promising route to large-scale calculations of the Rényi EE of interacting fermions [20–28]. However, the universal features of EE in 2D have remained out of reach for these methods. In the Grover method, one samples from uncorrelated replica configurations and the Rényi EE estimator suffers from rare events that dominate the statistical average. This problem becomes increasingly severe for larger entangling regions and interaction strengths. More elaborate DQMC methods of computing the Rényi EE [22,24] offer better controlled statistical errors. However, this comes at the price of increasing the effective number of degrees of freedom, making simulations more costly, and further requires special numerical stabilization techniques. The lack of adequate techniques has even sparked interest in alternative probes of fermion entanglement that offer superior efficiency [29,30].

In this work, we develop an improved method to compute the Rényi EE in DQMC that solves the above-mentioned sampling problem and enables us to achieve unprecedented precision. To do so, we leverage recent advancements in computing the Rényi EE in quantum spin systems via nonequilibrium work [31–34], originally inspired by [35], to develop an improved *equilibrium* method for DQMC simulations. Our approach harnesses the power of importance sampling by introducing an extended ensemble of Monte Carlo configurations in which the entangling region is allowed to fluctuate. Remarkably, the original formulation

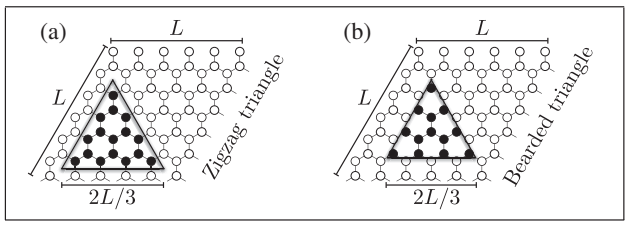

FIG. 1. (a) A triangular region on a 6×6 lattice with a zigzag edge. (b) A triangular region with a bearded edge.

by Grover admits such an extended ensemble that can be simulated efficiently using standard DQMC techniques.

In order to demonstrate the power of this technique, we use it to perform a comprehensive study of the logarithmic corrections to the area law in the half-filled honeycomb Hubbard model at $T = 0$. We first demonstrate the validity of our method by comparing to quasi-exact results obtained by density matrix renormalization group simulations (DMRG) [36]. Next we study the finite size scaling for two different triangular regions, see Fig. 1, in the semimetal phase and at the Gross-Neveu-Yukawa (GNY) critical point, where the latter shows an enhanced logarithmic contribution that depends on the type of entanglement cut. This is further demonstrated by tracking the logarithmic contribution as a function of the interaction strength throughout the semimetal phase and through the GNY point. Finally, we compute the half-system Rényi EE at large interaction strength deep in the Mott insulating phase, revealing the distinct logarithmic contribution due to Goldstone modes.

General method.—We consider the general framework of auxiliary-field DQMC simulations, which map interacting fermionic systems to free fermions coupled to a fluctuating Hubbard-Stratonovich (HS) field [37,38]. For a given HS field configuration s, one has access to the equal-time Green's function $G^s_{ij} = \langle c_i c^\dagger_j \rangle_s$. In Grover's method [20], the second Rényi EE, $S^A_2 = -\ln \mathrm{Tr}(\rho^2_A)$, can be computed considering two independent replica DQMC simulations with Green's functions $G^{s_1}_{ij}, G^{s_2}_{ij}$ and taking the average,

$$e^{-S^A_2} = \sum_{\{s_1\},\{s_2\}} P_{s_1} P_{s_2} \det\left(G^{s_1}_A G^{s_2}_A + (\mathbb{1} - G^{s_1}_A)(\mathbb{1} - G^{s_2}_A)\right). \tag{1}$$

Here G^s_A refers to the Green's function matrix that is restricted to the spatial region A, and P_s is the probability of configuration s. As previously mentioned, rare pairs of configurations (s_1, s_2) give large contributions to Eq. (1). To avoid this, we now show how to build correlations between the replica configurations such that the relevant phase space is better sampled, and in the process identify an improved Monte Carlo estimator for S^A_2.

Consider the distribution

$$Z_A = \sum_{\{s_1\},\{s_2\}} W_{s_1} W_{s_2} \det g^{s_1,s_2}_A, \tag{2}$$

where we define the Grover matrix $g^{s_1,s_2}_A = G^{s_1}_A G^{s_2}_A + (\mathbb{1} - G^{s_1}_A)(\mathbb{1} - G^{s_2}_A)$ and W_s is the standard DQMC weight (unnormalized) of configuration s. Equation (1) can now be written as $e^{-S^A_2} = Z_A/Z_\varnothing$, where $\varnothing$ refers to the empty set, containing a zero-dimensional Grover matrix with unit determinant. A highly efficient prescription for computing such partition function ratios was put forward in Ref. [31]. Following this, we now consider a generalized ensemble made up of entangling regions C, which are proper subsets of the region A [39]. Furthermore, we control the distribution with an external field λ that couples to the number of sites in the region C, denoted by N_C:

$$\mathcal{Z}(\lambda) = \sum_{C \subseteq A} \lambda^{N_C} (1-\lambda)^{N_A - N_C} Z_C, \tag{3}$$

where Z_C is given by Eq. (2) with A replaced by C. The ensemble in Eq. (3) is designed such that $\mathcal{Z}(0) = Z_\varnothing$ and $\mathcal{Z}(1) = Z_A$.

Given this, the ratio at two different values of λ can be computed via a simple reweighting

$$\frac{\mathcal{Z}(\lambda_j)}{\mathcal{Z}(\lambda_i)} = \left\langle \left(\frac{\lambda_j}{\lambda_i}\right)^{N_C} \left(\frac{1-\lambda_j}{1-\lambda_i}\right)^{N_A - N_C} \right\rangle_{\lambda_i}, \tag{4}$$

where the only stochastic variable here is N_C and the average is taken in the distribution according to λ_i. In this way we may introduce many intermediate values of λ in order to break up the overall exponentially small factor $(Z_A/Z_\varnothing) = [\mathcal{Z}(\lambda_1)/\mathcal{Z}(0)][\mathcal{Z}(\lambda_2)/\mathcal{Z}(\lambda_1)]\ldots[\mathcal{Z}(1)/\mathcal{Z}(\lambda_{N_\lambda})]$ into computationally manageable pieces [39].

A fundamental ingredient of our algorithm involves imbedding the Grover factor $\det(g^{s_1,s_2}_C)$ directly into the DQMC configurational weight, as required to sample from the distribution in Eq. (3). The inclusion of this factor is what effectively allows for importance sampling of the otherwise exponentially rare configurations appearing in Eq. (1). However, to include this factor in a manner that is both computationally efficient and numerically stable requires the resolution of a serious technical challenge, as we now describe.

Standard implementations of DQMC maintain an efficient computational complexity of $\mathcal{O}(N_\tau N^3_{\mathrm{site}})$ by avoiding the explicit computation of fermionic determinants [37,38]. This technique relies on access to the equal-time Green's function $G^s_{ij}(\tau)$ located at the imaginary time slice that is being updated. However, the Grover factor is always expressed in terms of Green's functions at a fixed imaginary time slice $G^s_{ij}(\theta)$, where observables are computed. Naïvely it would appear that the dependence of the configurational

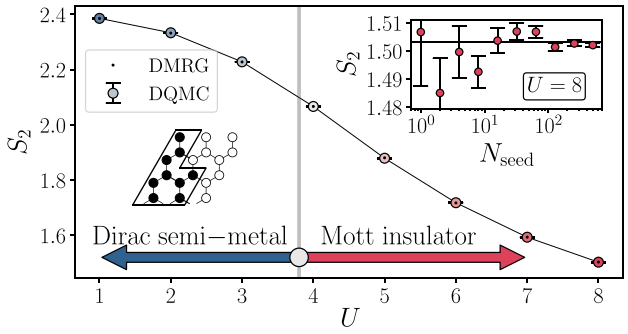

FIG. 2. The new DQMC computation of S_2 as compared to DMRG [36] for the system pictured. Here we use open boundaries in the x direction. The inset shows a closer look at the precise agreement at $U = 8$ using only a single value of $\lambda = 0.5$ and N_{seed} independent simulations.

weight (including the Grover factor) on two different sets of Green's functions would render the standard fast update formulas inapplicable, making simulations prohibitively costly. In the Supplemental Material [39] we show how this crucial technical hurdle is overcome by making use of imaginary time displaced Green's functions [40], a standard object in most DQMC simulations.

Model.—As a benchmark system for our new method we select a classic model of interacting fermions in two dimensions: the Hubbard model on the honeycomb lattice at half filling. The Hamiltonian is given by

$$H = -t\sum_{\langle i,j\rangle,\sigma}(c^{\dagger}_{i,\sigma}c_{j,\sigma} + \text{H.c.}) + U\sum_{i}\left(n_{i,\uparrow} - \frac{1}{2}\right)\left(n_{i,\downarrow} - \frac{1}{2}\right). \tag{5}$$

The restriction to half filling ensures the absence a sign problem, which equally applies to our generalized ensemble in Eq. (3). This model is known to host a semimetal phase with a gapless Dirac spectrum up to $U_c \approx 3.8$ [41,42], beyond which the system enters a Mott insulating antiferromagnetically ordered phase with Goldstone modes from the spontaneous breaking of spin rotation symmetry. The critical point at $U_c = 3.8$ is in the GNY chiral Heisenberg universality class [43].

In the gapless semimetal (SM) phase it is known that the Rényi EE of a triangular region with three sharp corners, depicted in Figs. 1(a) and 1(b), scales according to [6,7]

$$S_2 = \mathcal{A}L - 3a_2^{\text{SM}}(\pi/3)\ln(L) + \text{const.} \tag{6}$$

Here $a_2^{\text{SM}}(\pi/3) \approx 0.1324$ [44] is the universal coefficient from one $\pi/3$ corner with four free Dirac fermions (two spin and two valley). A similar scaling form is also expected to hold at the GNY critical point, albeit with an *unknown* value for the corner coefficient. We point out that unbiased numerical simulations are the only means of estimating universal corner contributions at interacting fixed points, as was previously done for the $2+1$d Ising, XY, and Heisenberg universality classes [45–50]. These studies support the notion of the corner coefficient as a measure of the number of effective low-energy degrees of freedom [51,52]. We are therefore interested in comparing the value at the GNY point to that of free Dirac fermions.

In the Mott insulating phase, the contribution from Goldstone modes to the Rényi EE for a smooth entangling cut, as depicted in Fig. 5, has a similar form [10]:

$$S_2 = \mathcal{A}L + \frac{N_g}{2}\ln(L) + \text{const.} \tag{7}$$

Here the logarithmic piece counts the number of Goldstone modes N_g, and comes with the opposite sign. Since the honeycomb Hubbard model exhibits a known corner term in the semi-metal phase, an unknown corner term at the critical point, and an expected contribution from $N_g = 2$ Goldstone modes in the Mott insulating phase, it serves as the perfect test bed to extract universal logs for the first time with our technique.

DQMC results.—We implemented the $T = 0$ projector DQMC algorithm (though our method can also be extended to finite temperature) with a symmetric Trotter decomposition and an SU(2) invariant HS transformation [37,38,53]. The calculations presented here used a Trotter step of $\Delta_\tau = 0.1$ unless otherwise noted [39].

We begin by comparing our method to quasi-exact results obtained by the DMRG method [36] on an $L = 3$ open cylinder as a function of U, shown in Fig. 2. Here we use a small Trotter step of $\Delta_\tau = 0.01$ and a ground state projection of $\theta = 10$ (2000 total Trotter slices). We find perfect agreement with the DQMC results, and already at this system size we can see the qualitative feature of the semimetal to Mott insulator transition near $U_c = 3.8$. We note that on larger system sizes more values of λ are needed such that adjacent distributions of N_C have good overlap. Details of the λ values used in this work are given in the Supplemental Material [39].

We now move on to confirm the expected behavior at $U = 1$. In the left panel of Fig. (3) we show DQMC results using the two different triangular regions depicted in Figs. 1(a) and 1(b). We have found that the ground state convergence of S_2 in the semimetal phase is heavily affected by the proximity to the Dirac point. We therefore use twisted boundary conditions in the x direction, where hoppings that wrap the x-boundary get multiplied by the phase $e^{i2\pi\phi}$ with $\phi = 0.1$ in order to shift the Dirac point [39]. We use projection times up to $\theta = 2L$ on our largest system sizes to ensure convergence. We find that both triangles give subleading logarithmic contributions that are consistent with the field theoretic value $a_2^{\text{SM}}(\pi/3) \approx 0.1324$ [44], namely, we find $a_2^{\text{SM}}(\pi/3) = 0.126(4), 0.136(2)$ for the zigzag and bearded triangles, respectively. This is shown in

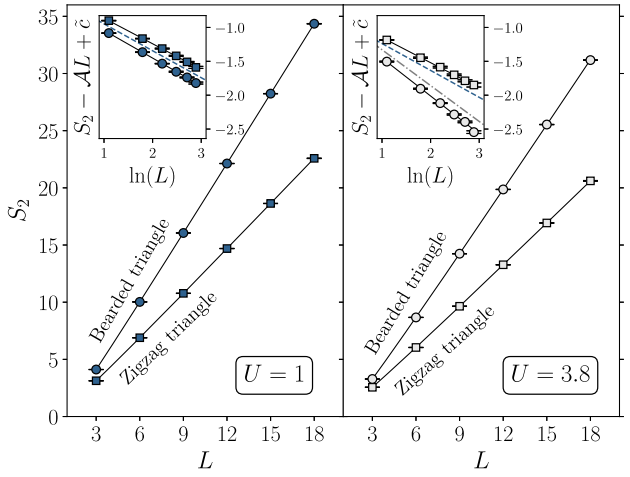

FIG. 3. Left panel: S_2 computed for both kinds of triangular regions depicted in Figs. 1(a) and 1(b) at $U = 1$ and twisted boundary conditions with $\phi = 0.1$. The inset shows the result of a three parameter fit to a linear plus log scaling and subtracting away the area law piece (a shift of $\tilde{c} = 1$ is given to the bearded triangle for clarity of comparison). The blue dashed line shows the field theory prediction for the semimetal phase. Right panel: the same analysis but for with $U = 3.8$ at the GNY point with $\phi = 0$. The bearded triangle shows an enhanced logarithmic contribution in this case. This is compared to the field theory value for free fermions plus a three-component boson shown by the gray dotted-dashed line in the inset.

the inset, where the fit to the area law term is subtracted away and the result is plotted versus $\ln(L)$.

Next in the right panel of Fig. 3 we perform the same analysis but with $U = 3.8$, at the GNY point. Here we find that ground state convergence is easier than in the semimetal phase and so we set $\phi = 0$ but still use $\theta = 2L$ on the largest system sizes. We interestingly find a difference in the logarithmic contributions between the zigzag and bearded triangles. The zigzag triangle gives a similar value to free Dirac fermions: $a_2^{\mathrm{GNY}}(\pi/3) = 0.124(5)$, while the bearded triangle shows an enhanced logarithmic contribution with $a_2^{\mathrm{GNY}}(\pi/3) = 0.187(12)$. It is appropriate to compare this with what is expected from free Dirac fermions plus a three component gapless boson (f + b) representing the Néel order parameter. The field theoretic value in this case gives $a_2^{\mathrm{f+b}}(\pi/3) \approx 0.1764$ [44], in the same range as the bearded triangle. While it is difficult to estimate the true value at the GNY point, which we expect to be less than the previously quoted field theory value [54], the fact that our finite size data produces a comparable value is encouraging and motivates us to investigate this logarithmic term in more detail.

We wish to now study the bearded triangle corner coefficient in detail as a function of U. In order to do this we use a much larger Trotter time step $\Delta_\tau = 0.5$, since we have found the logarithmic terms to be independent of the Trotter step [39]. We further fix $\theta = L$ (except $L = 3$ where

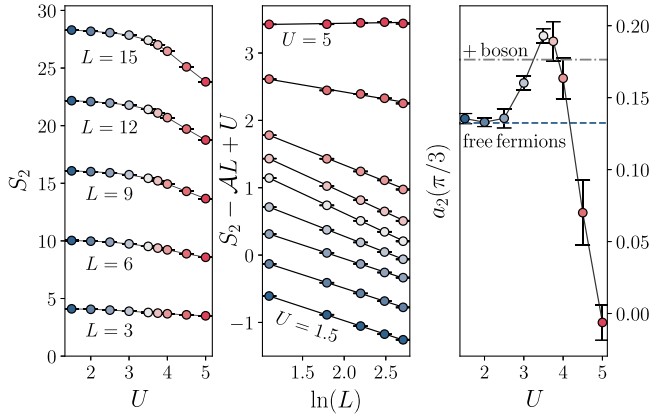

FIG. 4. Left panel: S_2 for bearded triangles depicted in Fig. 1(b) using $\Delta_\tau = 0.5$ and $\phi = 0.15$ as a function of U. Middle panel: The fit as a function of L performed for each value of U with the area law piece subtracted away, with a constant shift of U added for clarity. Right panel: The extracted corner coefficient as a function of U, showing an enhanced value at the GNY point.

we use $\theta = 2L$) and $\phi = 0.15$. The left panel of Fig. 4 shows the resulting S_2 data as a function of U. For each value of U we perform a fit as a function of L, then in the middle panel we reveal the logarithmic contribution by subtracting off the fitted area law piece. The resulting slopes are plotted in the rightmost panel, where we see clear agreement with the free fermion result throughout the semimetal phase with a pronounced enhancement at the GNY point followed by a sharp drop into the Mott insulating phase. The values at the GNY point are consistent with Fig. 3 even though here we have used twisted boundary conditions and a much larger Trotter step.

Finally, we further increase U into the antiferromagnetic Mott insulator phase where we expect to see a *positive* subleading logarithmic contribution coming from Goldstone modes, given by Eq. (7). Figure 5 shows the half-system

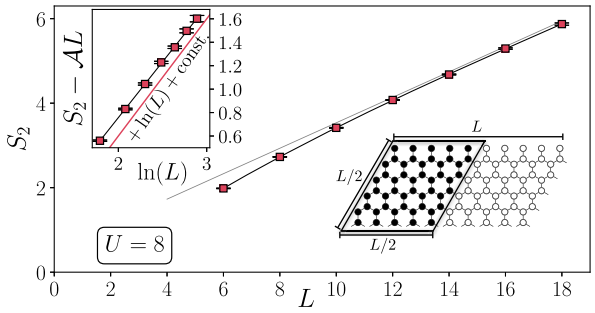

FIG. 5. Half-system entropy S_2 on rectangular systems as depicted, with $U = 8$. This plot is similar to Fig. 3, but now the subleading log term has the opposite sign, as can be seen by the slope in the inset. The thin line in the main panel helps to visualize the bend in the data coming from the logarithmic term. The coefficient of the log term counts the Goldstone modes with the coefficient $N_g/2$, here giving 0.95(5).

entropy on rectangular systems as shown in the figure with $U = 8$. We see a clear positive log with a coefficient in agreement with the contribution from two Goldstone modes.

Conclusions.—We introduced an equilibrium Monte Carlo estimator for the Rényi EE in interacting fermion systems that allows for importance sampling of the original estimator by Grover. We used this method to detect, for the first time, logarithmic corrections to the area law in a 2D model of interacting fermions. Importantly, we find that such logarithmic terms can be sensitive to the type of entanglement cut that is used.

Note added.—Since our method first appeared, it has been independently implemented and applied to several different fermionic models [55–57]. Additionally, building on our methodology, an even more efficient protocol was developed in [58] that obviates the need to sample over subset entangling regions.

We gratefully acknowledge William Witczak-Krempa for stimulating correspondence. R. O. and F. J. acknowledge funding from the Spanish MCI/AEI/FEDER (Grant No. PGC2018-101988-B-C21). Technical and human support provided by DIPC Supercomputing Center, where the main results were collected, is gratefully acknowledged. Additional resources were used from the XSEDE allocation NSF DMR-130040 using the Expanse cluster at SDSC.

*jonathan.demidio@dipc.org

[1] Christoph Holzhey, Finn Larsen, and Frank Wilczek, Geometric and renormalized entropy in conformal field theory, Nucl. Phys. **B424**, 443 (1994).
[2] G. Vidal, J. I. Latorre, E. Rico, and A. Kitaev, Entanglement in quantum critical phenomena, Phys. Rev. Lett. **90**, 227902 (2003).
[3] V. E. Korepin, Universality of entropy scaling in one dimensional gapless models, Phys. Rev. Lett. **92**, 096402 (2004).
[4] Pasquale Calabrese and John Cardy, Entanglement entropy and quantum field theory, J. Stat. Mech. (2004) P06002.
[5] J. Eisert, M. Cramer, and M. B. Plenio, Colloquium: Area laws for the entanglement entropy, Rev. Mod. Phys. **82**, 277 (2010).
[6] Eduardo Fradkin and Joel E. Moore, Entanglement entropy of 2d conformal quantum critical points: Hearing the shape of a quantum drum, Phys. Rev. Lett. **97**, 050404 (2006).
[7] H. Casini and M. Huerta, Universal terms for the entanglement entropy in $2 + 1$ dimensions, Nucl. Phys. **B764**, 183 (2007).
[8] H. F. Song, Nicolas Laflorencie, Stephan Rachel, and Karyn Le Hur, Entanglement entropy of the two-dimensional heisenberg antiferromagnet, Phys. Rev. B **83**, 224410 (2011).
[9] Ann B. Kallin, Matthew B. Hastings, Roger G. Melko, and Rajiv R. P. Singh, Anomalies in the entanglement properties of the square-lattice Heisenberg model, Phys. Rev. B **84**, 165134 (2011).
[10] Max A. Metlitski and Tarun Grover, Entanglement entropy of systems with spontaneously broken continuous symmetry, arXiv:1112.5166.
[11] Alexei Kitaev and John Preskill, Topological entanglement entropy, Phys. Rev. Lett. **96**, 110404 (2006).
[12] Michael Levin and Xiao-Gang Wen, Detecting topological order in a ground state wave function, Phys. Rev. Lett. **96**, 110405 (2006).
[13] Román Orús, Tzu-Chieh Wei, Oliver Buerschaper, and Maarten Van den Nest, Geometric entanglement in topologically ordered states, New J. Phys. **16**, 013015 (2014).
[14] R. Orús, T. C. Wei, Oliver Buerschaper, and Artur García-Saez, Topological transitions from multipartite entanglement with tensor networks: A procedure for sharper and faster characterization, Phys. Rev. Lett. **113**, 257202 (2014).
[15] Nicolas Laflorencie, Quantum entanglement in condensed matter systems, Phys. Rep. **646**, 1 (2016).
[16] Michael P. Zaletel, Roger S. K. Mong, and Frank Pollmann, Topological characterization of fractional quantum Hall ground states from microscopic Hamiltonians, Phys. Rev. Lett. **110**, 236801 (2013).
[17] W. Zhu, S. S. Gong, F. D. M. Haldane, and D. N. Sheng, Fractional quantum Hall states at $\nu = 13/5$ and $12/5$ and their non-Abelian nature, Phys. Rev. Lett. **115**, 126805 (2015).
[18] Benoit Estienne, Jean-Marie Stéphan, and William Witczak-Krempa, Cornering the universal shape of fluctuations, Nat. Commun. **13**, 287 (2022).
[19] Wei Zhu, Xiao Chen, Yin-Chen He, and William Witczak-Krempa, Entanglement signatures of emergent Dirac fermions: Kagome spin liquid and quantum criticality, Sci. Adv. **4**, eaat5535 (2018).
[20] Tarun Grover, Entanglement of interacting fermions in quantum Monte Carlo calculations, Phys. Rev. Lett. **111**, 130402 (2013).
[21] F. F. Assaad, T. C. Lang, and F. Parisen Toldin, Entanglement spectra of interacting fermions in quantum Monte Carlo simulations, Phys. Rev. B **89**, 125121 (2014).
[22] Peter Broecker and Simon Trebst, Rényi entropies of interacting fermions from determinantal quantum Monte Carlo simulations, J. Stat. Mech. (2014) P08015.
[23] Lei Wang and Matthias Troyer, Renyi entanglement entropy of interacting fermions calculated using the continuous-time quantum Monte Carlo method, Phys. Rev. Lett. **113**, 110401 (2014).
[24] Fakher F. Assaad, Stable quantum Monte Carlo simulations for entanglement spectra of interacting fermions, Phys. Rev. B **91**, 125146 (2015).
[25] Joaquín E. Drut and William J. Porter, Hybrid Monte Carlo approach to the entanglement entropy of interacting fermions, Phys. Rev. B **92**, 125126 (2015).
[26] Joaquín E. Drut and William J. Porter, Entanglement, noise, and the cumulant expansion, Phys. Rev. E **93**, 043301 (2016).
[27] Peter Broecker and Simon Trebst, Entanglement and the fermion sign problem in auxiliary field quantum Monte Carlo simulations, Phys. Rev. B **94**, 075144 (2016).
[28] Peter Broecker and Simon Trebst, Numerical stabilization of entanglement computation in auxiliary-field quantum

Monte Carlo simulations of interacting many-fermion systems, Phys. Rev. E **94**, 063306 (2016).
[29] Weilun Jiang, Bin-Bin Chen, Zi Hong Liu, Junchen Rong, Fakher F. Assaad, Meng Cheng, Kai Sun, and Zi Yang Meng, Many versus one: The disorder operator and entanglement entropy in fermionic quantum matter, SciPost Phys. **15**, 082 (2023).
[30] Zi Hong Liu, Weilun Jiang, Bin-Bin Chen, Junchen Rong, Meng Cheng, Kai Sun, Zi Yang Meng, and Fakher F. Assaad, Fermion disorder operator at Gross-Neveu and deconfined quantum criticalities, Phys. Rev. Lett. **130**, 266501 (2023).
[31] Jonathan D'Emidio, Entanglement entropy from nonequilibrium work, Phys. Rev. Lett. **124**, 110602 (2020).
[32] M. S. Block, Jonathan D'Emidio, and R. K. Kaul, Kagome model for a $\mathbb{Z}_2$ quantum spin liquid, Phys. Rev. B **101**, 020402(R) (2020).
[33] Jiarui Zhao, Yan-Cheng Wang, Zheng Yan, Meng Cheng, and Zi Yang Meng, Scaling of entanglement entropy at deconfined quantum criticality, Phys. Rev. Lett. **128**, 010601 (2022).
[34] Jiarui Zhao, Bin-Bin Chen, Yan-Cheng Wang, Zheng Yan, Meng Cheng, and Zi Yang Meng, Measuring Rényi entanglement entropy with high efficiency and precision in quantum Monte Carlo simulations, npj Quantum Mater. **7**, 69 (2022).
[35] Vincenzo Alba, Out-of-equilibrium protocol for Rényi entropies via the Jarzynski equality, Phys. Rev. E **95**, 062132 (2017).
[36] Matthew Fishman, Steven R. White, and E. Miles Stoudenmire, The ITensor software library for tensor network calculations, SciPost Phys. Codebases **4** (2022).
[37] E. Y. Loh and J. E. Gubernatis, Chapter 4—stable numerical simulations of models of interacting electrons in condensed-matter physics, in *Electronic Phase Transitions, Modern Problems in Condensed Matter Sciences*, edited by W. Hanke and Yu. V. Kopaev (Elsevier, New York, 1992), Vol. 32, pp. 177–235.
[38] F. F. Assaad and H. G. Evertz, World-line and determinantal quantum Monte Carlo methods for spins, phonons and electrons, in *Computational Many-Particle Physics*, edited by H. Fehske, R. Schneider, and A. Weiße (Springer, Berlin, Heidelberg, 2008), pp. 277–356.
[39] See Supplemental Material at http://link.aps.org/supplemental/10.1103/PhysRevLett.132.076502 for more details on the algorithm and the numerical simulations.
[40] M. Feldbacher and F. F. Assaad, Efficient calculation of imaginary-time-displaced correlation functions in the projector auxiliary-field quantum Monte Carlo algorithm, Phys. Rev. B **63**, 073105 (2001).
[41] Sandro Sorella, Yuichi Otsuka, and Seiji Yunoki, Absence of a spin liquid phase in the Hubbard model on the honeycomb lattice, Sci. Rep. **2**, 992 (2012).
[42] Fakher F. Assaad and Igor F. Herbut, Pinning the order: The nature of quantum criticality in the Hubbard model on honeycomb lattice, Phys. Rev. X **3**, 031010 (2013).
[43] Igor F. Herbut, Interactions and phase transitions on graphene's honeycomb lattice, Phys. Rev. Lett. **97**, 146401 (2006).
[44] Johannes Helmes, Lauren E. Hayward Sierens, Anushya Chandran, William Witczak-Krempa, and Roger G. Melko, Universal corner entanglement of Dirac fermions and gapless bosons from the continuum to the lattice, Phys. Rev. B **94**, 125142 (2016).
[45] Rajiv R. P. Singh, Roger G. Melko, and Jaan Oitmaa, Thermodynamic singularities in the entanglement entropy at a two-dimensional quantum critical point, Phys. Rev. B **86**, 075106 (2012).
[46] Ann B. Kallin, Katharine Hyatt, Rajiv R. P. Singh, and Roger G. Melko, Entanglement at a two-dimensional quantum critical point: A numerical linked-cluster expansion study, Phys. Rev. Lett. **110**, 135702 (2013).
[47] A. B. Kallin, E. M. Stoudenmire, P. Fendley, R. R. P. Singh, and R. G. Melko, Corner contribution to the entanglement entropy of an o(3) quantum critical point in $2+1$ dimensions, J. Stat. Mech. 06 (2014) P06009.
[48] Johannes Helmes and Stefan Wessel, Entanglement entropy scaling in the bilayer Heisenberg spin system, Phys. Rev. B **89**, 245120 (2014).
[49] E. M. Stoudenmire, Peter Gustainis, Ravi Johal, Stefan Wessel, and Roger G. Melko, Corner contribution to the entanglement entropy of strongly interacting o(2) quantum critical systems in $2+1$ dimensions, Phys. Rev. B **90**, 235106 (2014).
[50] Johannes Helmes and Stefan Wessel, Correlations and entanglement in quantum critical bilayer and necklace XY models, Phys. Rev. B **92**, 125120 (2015).
[51] Pablo Bueno, R. C. Myers, and William Witczak-Krempa, Universality of corner entanglement in conformal field theories, Phys. Rev. Lett. **115**, 021602 (2015).
[52] Pablo Bueno and Robert C. Myers, Corner contributions to holographic entanglement entropy, J. High Energy Phys. 08 (2015) 068.
[53] F. F. Assaad, Su(2)-spin invariant auxiliary field quantum Monte-Carlo algorithm for Hubbard models, in *High Performance Computing in Science and Engineering '98*, edited by Egon Krause and Willi Jäger (Springer, Berlin Heidelberg, 1999), pp. 105–111.
[54] William Witczak-Krempa (private communication).
[55] Yuan Da Liao, Gaopei Pan, Weilun Jiang, Yang Qi, and Zi Yang Meng, The teaching from entanglement: 2D SU(2) antiferromagnet to valence bond solid deconfined quantum critical points are not conformal, arXiv:2302.11742.
[56] Gaopei Pan, Yuan Da Liao, Weilun Jiang, Jonathan D'Emidio, Yang Qi, and Zi Yang Meng, Stable computation of entanglement entropy for two-dimensional interacting fermion systems, Phys. Rev. B **108**, L081123 (2023).
[57] Zi Hong Liu, Yuan Da Liao, Gaopei Pan, Menghan Song, Jiarui Zhao, Weilun Jiang, Chao-Ming Jian, Yi-Zhuang You, Fakher F. Assaad, Zi Yang Meng, and Cenke Xu, Disorder operator and Rényi entanglement entropy of symmetric mass generation, arXiv:2308.07380.
[58] Yuan Da Liao, Controllable incremental algorithm for entanglement entropy and other observables with exponential variance explosion in many-body systems, arXiv:2307.10602.